Pseudospin Paramagnons and the Superconducting Dome in Magic Angle Twisted Bilayer Graphene

Chunli Huang, Nemin Wei, Wei Qin, and Allan H. MacDonald

Pseudospin Paramagnons and the Superconducting Dome
in Magic Angle Twisted Bilayer Graphene

Chunli Huang, Nemin Wei, Wei Qin, and Allan H. MacDonald

Department of Physics, University of Texas at Austin, Austin TX 78712

(Dated: July 26, 2022)

We present a theory of superconductivity in twisted bilayer graphene in which attraction is generated between electrons on the same honeycomb sublattice when the system is close to a sublattice polarization instability. The resulting Cooper pairs are spin-polarized valley-singlets. Because the sublattice polarizability is mainly contributed by interband fluctuations, superconductivity occurs over a wide range of filling fraction. It is suppressed by i) applying a sublattice polarizing field (generated by an aligned BN substrate) or ii) changing moiré band filling to favor valley polarization. The enhanced intrasublattice attraction close to sublattice polarization instability is analogous to enhanced like-spin attraction in liquid ^{3}He near the melting curve and the enhanced valley-singlet repulsion close to valley-polarization instabilities is analogous to enhanced spin-singlet repulsion in metals that are close to a ferromagnetic instability. We comment on the relationship between our pseudospin paramagnon model and the rich phenomenology of superconductivity in twisted bilayer and multilayer graphene.

Introduction:– Many properties of moiré superconductors in twisted multilayer graphene systems [1–3] like the microscopic origin of the T_c dome and the large ratio of transition temperature over the Fermi temperature ($T_c/T_F \sim 0.1$) are still not well understood. However, possible explanations for superconductivity are increasingly constrained by experimental data [4–17]. The normal state properties revealed by the weak-field Hall effect and magnetoresistance oscillations [14] are particularly telling; the strongest superconductivity occurs within the moiré band filling interval $\nu \in (-3, -2)$, within which the system has a hole-like Fermi surfaces surrounding $|\nu|-2$ states per moiré period. The implied Fermi surface reconstruction points to symmetry breaking that depopulates two of four spin/valley flavors, an interpretation that is reinforced by Landau fans that are only doubly degenerate for $\nu \in (-3, -2)$ in spite of the systems four-fold spin/valley band degeneracy. The normal state symmetry breaking provides a natural explanation for large in-plane critical magnetic fields [15] that are $\sim 2-3$ times larger than the Clogston-Chandrashekar limit of spin-singlet superconductors. As summarized in Fig. 1, superconductivity is suppressed as ν approaches -3 and as ν approaches -2, filling factors at which the system is known to tend toward valley-ordered states, forming a dome in the system's (T, ν) phase diagram that is reminiscent of those observed in cuprate superconductors. For example, the superconducting critical temperature T_c of device 1 in Ref. [6] is peaked at $\nu \sim -2.4$, and vanishes near $\nu \to -2.6$ on the low-filling-factor side and near $\nu \to -2.2$ on the high filling factor side. The suppression of superconductivity on the low-filling factor side occurs in spite of an increasing Fermi level density-of-states, and therefore argues against a mechanism, like phonon-dressing, in which the pairing glue is external to the electron system. Superconductivity actually seems to be suppressed when the Fermi level is close to a the flat valence band van Hove singularity energy [2, 12]. These experimental observations point to an electronic pairing mechanism.

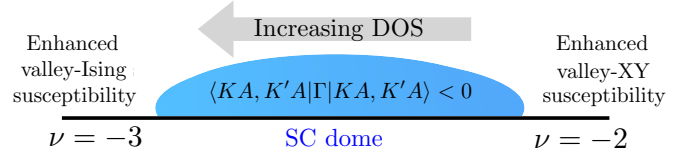In this Letter, we argue that the superconducting properties of MATBG are consistent with a sublattice-pseudospin

FIG. 1. Exchange-enhanced sublattice pseudospin polarizatibility leads to an attractive intrasublattice interaction that can support spin-triplet, valley-singlet superconductors across a wide range of moiré band filling fraction ν. Superconductivity is suppressed when ν is tuned close to valley polarization instabilities and when the density-of-states (DOS) is small.

paramagnon pairing mechanism, and interpret the shape of the superconducting dome in terms of sublattice and valley paramagnons. Our main message is summarized in Fig. 1.

Pseudospin-paramagnons (PPM) and fermion pairing:- Our theory of MATBG superconductivity is guided by experiments [14, 15] and inspired by what is known about the relationship between fermion pairing in liquid ^{3}He and the strongly enhanced paramagnetic spin susceptibilities that appear near the solidification curve [21]. The enhanced susceptibility leads to a low-frequency neutral excitation spectrum that is dominated by *paramagon* peaks, damped collective modes that generates a strong attractive interaction between like-spin nuclei, and leads to anisotropic spin-triplet Anderson-Brinkman-Morel [22] superfluidity. Spin-fluctuation mediated superfluidity in ^{3}He is succinctly captured by the paramagnon model, which uses a single exchange-interaction parameter I to describe the enhanced spin susceptibility [23].

Unlike nuclei in ^{3}He, which possess only a spin degree of freedom, flat-band electrons in MATBG possess a spin(s)×valley(τ)×sublattice(σ) pseudospin octet that generates eight distinct states for each momentum and an abundance of potential pairing channels that has to be winnowed. Some progress can be achieved by taking note of the time-reversal symmetry property $\epsilon_K(\boldsymbol{k}) = \epsilon_{K'}(-\boldsymbol{k})$, which strongly favors
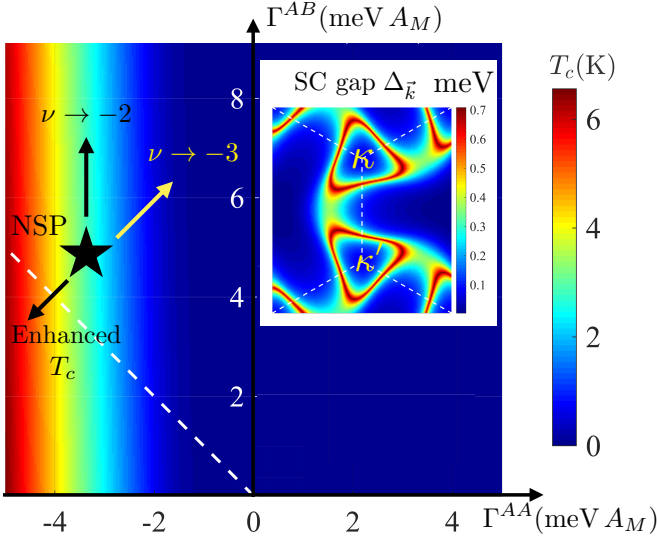
FIG. 2. T_c v.s. Γ^{AA} and Γ^{AB}. $A^a = (\Gamma^{AA} - \Gamma^{AB})/2$ is attractive and strong in nearly sublattice polarized (NSP) metals, whereas $A^s = (\Gamma^{AA} + \Gamma^{AB})/2$ is repulsive, but weak if screening is strong. Superconductivity occurs at low temperature when Γ^{AA} is attractive, even though Γ^{AB} is repulsive. The physically accessible parameter range above the dashed white $A^s = 0$ line includes superconductivity states. The inset plots the pairing self-energy $\Delta_{\vec{k}}$ vs. $\boldsymbol{k}$ in the moiré Brillouin-zone for a continuum model with $t_{AA}/t_{AB} = 0.7$, at $\theta = 1.1°$, at $\nu = -2.4$ [18]. $\Delta_{\boldsymbol{k}}$ is largest near the normal state Fermi surfaces centered on κ, κ'. When the system is close to a valley-Ising instability (near -3) or when it is sublattice polarized (near $\nu = +3$) [19, 20], $\nu = +1$ [12]), Γ^{AA} will increase and superconductivity will weaken. When A^s is decreased by the acoustic-phonon mediated interaction and/or screening of the long-range Coulomb interactions, T_c is enhanced. These trends are indicated by arrows and discussed in the main text.

Cooper pairing between electrons in opposite valleys K and K' ($\epsilon_K(\boldsymbol{k}) \neq \epsilon_K(-\boldsymbol{k})$). If we assume [14, 15] that the normal state for $\nu < -2$ is ferromagnetic (in spin), we can conclude that the Cooper pairs must be spin-polarized valley-singlets. That still leaves the sublattice pseudospin, and the need to overcome the strong sublattice independent Coulomb repulsion. A route to superconductivity is provided by the properties of the flatband spinors which imply, as illustrated in Fig. 2, that superconductivity occurs when the intrasublattice interaction is attractive ($\Gamma^{AA} < 0$) even if the intersublattice interaction is strongly repulsive ($\Gamma^{AB} > 0$) [24]. This property of magic-angle superconductivity is analogous to the robustness of spin-triplet superconductivity against repulsive opposite-spin interactions in systems with weak spin-orbit coupling [25], and can be traced to the D_6 point-group symmetry of the band Hamiltonian which decouples like-sublattice and unlike-sublattice pairing in the linearized gap equation.

We show below that intrasublattice attraction is generated when the system is close to a spontaneous sublattice polarization instability. This instability is common in graphene multilayers because sublattice polarization simplifies the spinor content of occupied states and increases exchange energies

[26, 27]. The same analysis that shows that sublattice PPM bolster superconductivity, shows that valley PPM are obstructive.

Sublattice-Dependent Effective Interactions:-. The reduced pairing Hamiltonian for spin $\uparrow$ electrons in opposite valleys is

$$H_{\text{red}} = \sum_{\boldsymbol{k}\boldsymbol{k}',\sigma_i} \left[\Gamma_{\boldsymbol{k}\boldsymbol{k}'}(\sigma_1\sigma_4; \sigma_2\sigma_3) \right.$$
$$\left. \times c^\dagger_{\boldsymbol{K}+\boldsymbol{k}'\sigma_1\uparrow} c^\dagger_{-\boldsymbol{K}-\boldsymbol{k}'\sigma_2\uparrow} c_{-\boldsymbol{K}-\boldsymbol{k}\sigma_3\uparrow} c_{\boldsymbol{K}+\boldsymbol{k}\sigma_4\uparrow} \right], \quad (1)$$

where Γ is the particle-particle channel irreducible 4-point vertex function estimated below [28, 29], $\boldsymbol{k}$ labels a state in the moiré valence band, and $\sigma = (A, B)$ labels sublattice. As we explain below, the PPM contributions to Γ are dominantly diagonal in sublattice at each vertex. This property motivates a model in which the dependence of Γ on $\boldsymbol{k}, \boldsymbol{k}'$ is neglected and C_2 symmetry is recognized:

$$\Gamma_{\boldsymbol{k}\boldsymbol{k}'}(\sigma_1\sigma_4; \sigma_2\sigma_3) \rightarrow \delta_{\sigma_1,\sigma_4}\delta_{\sigma_2,\sigma_3}\left[\Gamma^{AA}\delta_{\sigma_1,\sigma_2} + \Gamma^{AB}\delta_{\sigma_1,-\sigma_2} \right].$$
$$(2)$$

As illustrated in Fig. 2, superconductivity occurs in this model when the same sublattice effective interaction Γ^{AA} is attractive. The superconductivity gap is approximately uniform on the valley-projected FS (centered around κ and κ'), as shown in the inset. T_c is not suppressed by repulsive Γ^{AB} interactions because the susceptibility for pairs on opposite sublattices averages to zero on the Fermi surface. Motivated by this observation, we now address the relationship of Γ^{AA} to PPMs.

Recognizing that the computation of Γ from first-principles is a formidable challenge even in relatively simple systems [25, 30], we follow a phenomenological approach similar in spirit to that employed successfully in ^{3}He [31]. In that case spin-rotational invariance allows the spin-dependent effective interaction to be parameterized by just two scattering amplitudes, one each for the spin-symmetric and spin antisymmetric channel, (i.e. $\Gamma = A^s + A^a \boldsymbol{s_1} \cdot \boldsymbol{s_2}$ [21]). In MATBG, the Hamiltonian is not invariant under rotations of the sublattice pseudospins. When the system is close to a sublattice-polarization instability, however, effective interactions that are diagonal in sublattice dominate and the analogous expressions are

$$\Gamma^{AA} = A^s + A^a , \quad \Gamma^{AB} = A^s - A^a. \quad (3)$$

We estimate A^s and A^a by assuming a simple δ-function interaction model in order to sum the Feynman diagrams specified by Fig. 3. The irreducible vertex function Λ accounts for both direct and exchange scattering (i.e. generalized-random-phase approximation) generated by u_0 and $u_\perp$. u_0 is the fully symmetric Coulomb interaction while the valley-exchange scattering term $u_\perp > 0$ breaks independent spin-rotation symmetry in opposite valleys and selects the spin-ferromagnet over other possibilities as the flavor-polarized normal state. [32]

Ignoring the Berk-Schrieffer transverse fluctuation diagram in Fig. 3, see [18] for an in-depth discussion, we find that

$$A^s = \frac{1}{2}(T^{\tau_0\sigma_0} - T^{\tau_z\sigma_0}) , \quad A^a = \frac{1}{2}(T^{\tau_0\sigma_z} - T^{\tau_z\sigma_z}), \quad (4)$$
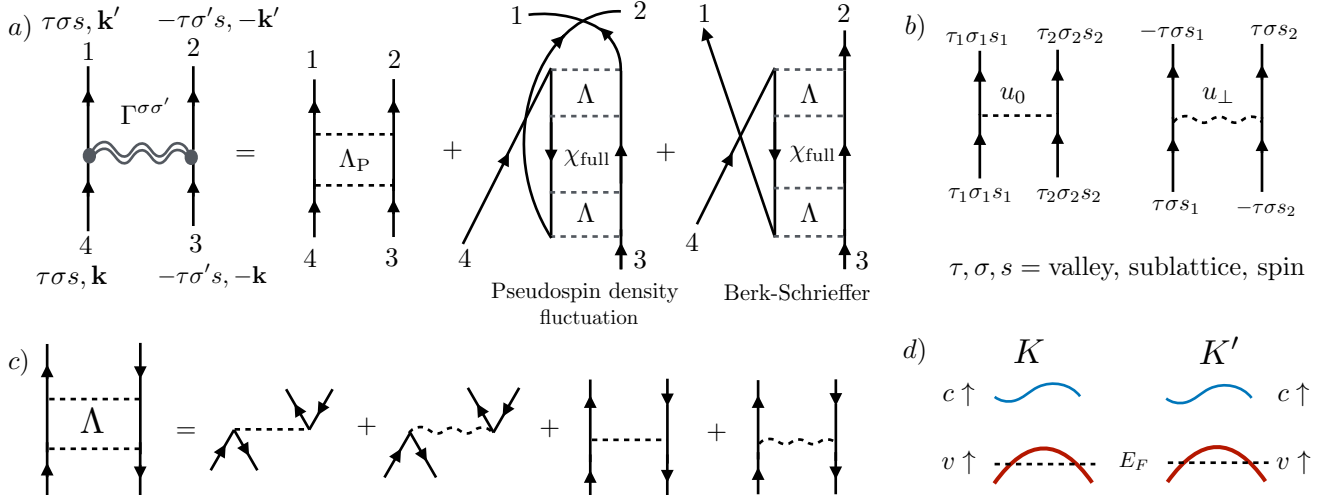
FIG. 3. a) The interaction potential Γ relevant to superconductivity has three contributions [28, 29]: a particle-particle vertex function Λ_P, a double-crossing diagram and the Berk-Schrieffer (single-crossing) diagram. The crossing diagrams relate Γ to paramagnon interactions that diverge at particle-hole instabilities. b) $u_0 > 0$ is a pseudospin-independent density-density interaction and $u_\perp > 0$ is an inter-valley scattering potential. c) The particle-hole vertex function Λ consists of the direct and exchange scattering terms from both u_0 and $u_\perp$. d) Schematic Fermi surface for $-3 < \nu < -2$ where $c(v)$ are the spin and valley projected conduction (valence) band.

where for small paramagnon wave vector $\boldsymbol{q} = \boldsymbol{k} - \boldsymbol{k}'$,

$$T^{\tau_0 \sigma_0} = \frac{1}{2} \frac{(3u_0 - u_\perp)}{1 + (3u_0 - u_\perp)\chi^{K\sigma_0, K\sigma_0}_{\boldsymbol{k}-\boldsymbol{k}',\omega}/2}, \tag{5}$$

$$T^{\tau_z \sigma_0} = -\frac{1}{2} \frac{u_0 - u_\perp}{1 - (u_0 - u_\perp)\chi^{K\sigma_0, K\sigma_0}_{\boldsymbol{k}-\boldsymbol{k}',\omega}/2}, \tag{6}$$

$$T^{\tau_0 \sigma_z} = -\frac{1}{2} \frac{u_0 + u_\perp}{1 - (u_0 + u_\perp)\chi^{K\sigma_z, K\sigma_z}_{\boldsymbol{k}-\boldsymbol{k}',\omega}/2}, \tag{7}$$

$$T^{\tau_z \sigma_z} = -\frac{1}{2} \frac{u_0 - u_\perp}{1 - (u_0 - u_\perp)\chi^{K\sigma_z, K\sigma_z}_{\boldsymbol{k}-\boldsymbol{k}',\omega}/2}, \tag{8}$$

Here $\chi^{O,O^\dagger}_{\boldsymbol{q},\omega=0}$ is a bare susceptibility for pseudospin polarization O. We discuss the valley-diagonal, sublattice even ($\chi^{K\sigma_0, K\sigma_0}_{\boldsymbol{q},\omega=0}$) and sublattice odd ($\chi^{K\sigma_z, K\sigma_z}_{\boldsymbol{q},\omega=0}$) susceptibilities further below.

The random phase sums decouple contributions that are proportional to different products of valley and sublattice Pauli matrices (τ_0 or τ_z and σ_0 or σ_z) of the interacting particle-hole pairs and yield pseudospin-dependent interactions that are sums of the four different geometric series. In each of the $T^{\tau_a \sigma_b}$'s a bare interaction is modified by a dressing factor (i.e. denominator) identical to the one that modifies the corresponding susceptibility. For the valley and sublattice independent interaction $T^{\tau_0 \sigma_0}$ the bare interaction is dominated by the bare repulsive Coulomb interaction u_0 and the modification is suppression due to static screening. For all other interaction channels, the dominant bare contribution is an attractive exchange contribution and the modification factor yields enhancement. At lowest order $\Gamma^{AA} = u_0 - u_\perp$ and $\Gamma^{AB} = u_0$ are both repulsive. Superconductivity is possible when $T^{\tau_0 \sigma_z}$, which contributes attractively to Γ^{AA}, has much larger enhancement factors than $T^{\tau_z \sigma_0}$ and $T^{\tau_z \sigma_z}$, both

of which contribute repulsively and diverge at valley polarization instabilities. We conclude that attractive intra-sublattice effective interactions, and hence superconductivity, is likely when the system is close to a valley-independent sublattice polarization instability but far from a valley-polarization instabilities.

The Superconducting Dome:–. We are now in a position to explain how the distinct filling factor dependencies of the different $T^{\tau_a \sigma_b}$'s forms the superconducting dome. An enhanced sublattice polarization susceptibility, which strengthens an attractive interaction, is present when the corresponding Stoner criterion $(u_0 + u_\perp)\chi^{K\sigma_z, K\sigma_z}_{\boldsymbol{q},\omega=0}/2 = 1$, is nearly satisfied. Repulsive interactions are strengthened when one of the valley polarization susceptibilities, with Stoner criteria $(u_0 - u_\perp)\chi^{K\sigma_0, K\sigma_0}_{\boldsymbol{q},\omega=0}/2 = 1$ or $(u_0 - u_\perp)\chi^{K\sigma_z, K\sigma_z}_{\boldsymbol{q},\omega=0}/2 = 1$, are close to being satisfied. Because $u_0 + u_\perp$ is larger than $u_0 - u_\perp$ the attractive $\tau_0 \sigma_z$ channel interaction is always stronger than the repulsive $\tau_z \sigma_z$ channel. Physically, the $\tau_0 \sigma_z$ susceptibility is enhanced and the $\tau_z \sigma_z$ susceptibility suppressed by $u_\perp$ because its exchange energy is maximized when opposite valleys have identical sublattice polarization. The competition between normal and superconducting states is therefore between the sublattice polarization Stoner criteria, which involves the $\chi^{K\sigma_z, K\sigma_z}_{\boldsymbol{q},\omega=0}$ polarization, and the valley polarization Stoner criterion, which involves $\chi^{K\sigma_0, K\sigma_0}_{\boldsymbol{q},\omega=0}$. Because of $C_2 T$ symmetry (where T is a spinless time-reversal symmetry) these two polarizations have very distinct dependencies on band filling. In particular $\chi^{K\sigma_z, K\sigma_z}_{\boldsymbol{q}=0,\omega=0}$ does not have an intraband contributions because the expectation value of σ_z is zero in all moiré band states. Its value is therefore not related to peaks in the band density-of-states and, as illustrated in Fig. 3d, should instead be larger closer to $\nu = -2$ where the majority spins are nearly

half-filled and the interband transition phase space is therefore largest. On the other hand, $\chi^{K\sigma_0,K\sigma_0}_{q\to0,\omega=0}$ is proportional to the Fermi level density of states and increases rapidly as $|\nu| - 2$ increases and the Fermi level approaches the Van Hove peak in the valence moiré band. We attribute the suppression of superconductivity on the large $|\nu| - 2$ side of the superconducting dome to the increasingly strong repulsive interaction contribution to A^s from $T^{\tau_z\sigma_0}$, which is proportional to the valley polarization susceptibility enhancement factor and suppresses superconductivity, as indicated in Fig. 2. On the other hand, we attribute the suppression of superconductivity on the small $|\nu| - 2$ side of the dome to the decreasing Fermi-level density-of-states.

We emphasize that our picture of superconductivity in graphene moiré superlattice requires that the normal state is nearly sublattice polarized metal over a wide range of filling fraction. Enhanced sublattice polarization, and sometimes sublattice polarization instabilities, are in fact common in all graphene multilayer electron gas systems [26]. For example, neutral Bernal bilayer graphene has $\sigma_z s_z$ order, *i.e.* spin-dependent sublattice-polarization in the antiferromagnetic state [27]. In twisted bilayers the gaps between flat and remote bands open an opportunity for flavor polarization and hence for sublattice polarization not only near neutrality but also near integer ν. In moiré flat bands itinerant exchange energies favor maximum spin-polarization before orbital-polarization, allowing the majority spin projected conduction and valence bands to mix and produce finite sublattice polarization over a wide range of filling fraction.

Summary and Discussions:– Paramagnon-mediated pairing physics in MATBG is enriched by the relevance of spin, valley, and sublattice pseudospins. Because the valley-projected bands are not time-reversal invariant, pairing is likely to occur between time-reversal partner states in opposite valleys and yield valley-singlets. We have shown that valley-singlet superconductivity occurs in MATBG when the effective interaction between electrons on the same sublattice is attractive, and that this condition is satisfied when the system is close to a sublattice-polarization instability, but far from a valley-polarization instability. There is no need for the interaction between electrons on opposite sublattice, or the total interaction summed over sublattices, to be attractive. Enhanced intrasublattice attraction close to sublattice polarization instabilities is analogous to the enhanced like-spin attraction in ^{3}He [22] near the melting curve, and enhanced valley-singlet repulsion close to valley-polarization instabilities is analogous to enhanced spin-singlet repulsion [23]in metals that are close to a ferromagnetic instability [33]. Together these two effects explain the prominent superconducting domes seen in most MATBG samples inside the filling factor interval $\nu \in (2, 3)$.

We now comment on other aspects of the phenomenlogy of MATBG superconductivity seen through the pseudospin paramagnon lens:

i) *Influence of Boron-Nitride (hBN) Alignment:*– Aligned hBN induces a finite sublattice polarization in a graphene sheet, and weakens sublattice pseudospin fluctuations. Since all other contributions to the intrasublattice interaction are repulsive, this theory predicts that superconductivity is suppressed by hBN alignment, in agreement with current experimental findings.

ii) *Coulomb screening:*– When MATBG devices are surrounded by nearby material that is conducting [6, 10, 34] or has a large dielectric constant [35], insulating states at integer filling factors become less prominent in the phase diagram and superconductivity is found over a broader range of filling factors. Insulating states are understood in terms of exchange-splitting between bands associated with different flavor states that is larger than the flatband bandwidth. Since the exchange splittings are dominated by the Coulomb interaction u_0, they are expected to be reduced by enhanced environmental screening. The reduction in insulating state gaps seen experimentally is therefore expected. On the other hand, the net attractive interaction from sublattice paramagnon scales with the intervalley-exchange interaction $u_\perp$, which should not be influenced by environmental screening. In addition the enhancement factors in $T^{\tau_0\sigma_z}$ and $T^{\tau_z\sigma_z}$, which together contribute attractively to Γ^{AA}, both involve the $\chi^{K\sigma_z,K\sigma_z}_{q,\omega}$ susceptibility which does not have a $q = 0$ Fermi surface contribution. $\chi^{K\sigma_z,K\sigma_z}_{q,\omega}$ is instead dominated by inter-band fluctuations that are less sensitive to remote screening. On the other hand, $T^{\tau_0\sigma_0}$, the repulsive screened Coulomb interaction, is certainly weakened by enhanced dielectric screening. The net result of enhanced remote screening could therefore be to enhance superconductivity, as sometimes observed experimentally. Although both superconductivity and insulating behavior require interactions, remote screening influences only u_0, and can therefore have opposite influences on the two states.

iii) *Superconductivity near $\nu = 0$:*– Although superconductivity is most robustly observed for $\nu \in (2, 3)$, the hole-like and electron-like Fermi surfaces on opposite side of $\nu = 0$ also sometimes host superconductivity as shown in Ref. [5]. Since our proposed theory of superconductivity between $-3 < \nu < -2$ only involves states in a spin-projected Hilbert space (*c.f.* Fig. 3d), it can be extended to $-1 < \nu < +1$ by assuming an identical pairing mechanism occurs in in both spin projected Hilbert spaces. This state would be similar to the equal spin pairing state in ^{3}He. The stronger superconductivity for $-3 < \nu < -2$, could be attributed to band-renormalizations that flatten bands away from half-filling. [16, 36–38].

iv) *Particle-hole asymmetry of superconductivity:*– Experiment shows that the tendency toward valley polarization, which opposes superconductivity, is stronger for electron-doped than for hole-doped MATBG. This tendency is due in part to conduction bands that are less dispersive than the valence bands, and have a different shape [16, 36–38]. It is quite likely that the normal state on the electron-doped side is a sublattice ferromagnet, or nearly so, as is supported by the observation of the AHE over a wide range of filling factors near $\nu = 3$ in devices with aligned hBN [19, 20] and in $\nu = 1$ [12] without aligned hBN. In addition, the valley PPMs that suppress superconductivity are certain to be stronger on the electron-doped

side.

v) *Phonon mediated pairing* [39–44]:– Brillouin Zone center Γ optical (acoustic) phonon mediated interactions are outside (inside) the interaction parameter space spanned by Γ^{AA} and Γ^{AB}. Explicit gap equation solutions [40, 41] show that optical phonons can induce superconductivity if the repulsive Coulomb interaction is somehow strongly suppressed. When the acoustic phonon propagator is not screened by electrons, it leads to a ν-independent attraction $\Gamma^{AA} = A^s \sim -0.5\text{meV} \cdot A_M$ [41] that is too small to explain the superconductivity dome. As shown in Fig. 2, since acoustic phonons reduce A_s [45], they can nevertheless play a role in enhancing T_c.

The pseudospin parmagnon is able to account for many aspects of the rich phenomenology of MATBG, including the mismatch between conditions that favor superconductivity and the anomalous Hall effect, the influence of enhanced remote screening, and particle-hole asymmetry. Our proposal can be tested by systematically studying how encapsulating hBN alignment and remote screening influence superconductivity. It is interesting to contrast superconductivity in MATBG with the recently discovered [46–48] superconductivity in multilayer graphene, which also has spin, valley, and sublattice pseudospins and has the advantage of simpler underlying electronic structure. In multilayer graphene without moiré potential superconductivity appears to be enhanced by proximity to a transition that occurs between unbroken-symmetry and partially flavor polarized states. The difference between the two cases may lie in the underlying physics that controls pseudospin polarization instabilities and the shape of the Fermi surface [49, 50].

[1] Y. Cao, V. Fatemi, S. Fang, K. Watanabe, T. Taniguchi, E. Kaxiras, and P. Jarillo-Herrero, "Unconventional superconductivity in magic-angle graphene superlattices," *Nature*, vol. 556, no. 7699, pp. 43–50, 2018.

[2] J. M. Park, Y. Cao, K. Watanabe, T. Taniguchi, and P. Jarillo-Herrero, "Tunable strongly coupled superconductivity in magic-angle twisted trilayer graphene," *Nature*, vol. 590, no. 7845, pp. 249–255, 2021.

[3] J. M. Park, Y. Cao, L. Xia, S. Sun, K. Watanabe, T. Taniguchi, and P. Jarillo-Herrero, "Magic-angle multilayer graphene: A robust family of moir\'e superconductors," *arXiv preprint arXiv:2112.10760*, 2021.

[4] M. Yankowitz, S. Chen, H. Polshyn, Y. Zhang, K. Watanabe, T. Taniguchi, D. Graf, A. F. Young, and C. R. Dean, "Tuning superconductivity in twisted bilayer graphene," *Science*, vol. 363, no. 6431, pp. 1059–1064, 2019.

[5] X. Lu, P. Stepanov, W. Yang, M. Xie, M. A. Aamir, I. Das, C. Urgell, K. Watanabe, T. Taniguchi, G. Zhang, *et al.*, "Super-

[6] Y. Saito, J. Ge, K. Watanabe, T. Taniguchi, and A. F. Young, "Independent superconductors and correlated insulators in twisted bilayer graphene," *Nature Physics*, vol. 16, no. 9, pp. 926–930, 2020.

[7] H. Polshyn, M. Yankowitz, S. Chen, Y. Zhang, K. Watanabe, T. Taniguchi, C. R. Dean, and A. F. Young, "Large linear-in-temperature resistivity in twisted bilayer graphene," *Nature Physics*, vol. 15, no. 10, pp. 1011–1016, 2019.

[8] Y. Cao, D. Chowdhury, D. Rodan-Legrain, O. Rubies-Bigorda, K. Watanabe, T. Taniguchi, T. Senthil, and P. Jarillo-Herrero, "Strange metal in magic-angle graphene with near planckian dissipation," *Physical review letters*, vol. 124, no. 7, p. 076801, 2020.

[9] F. K. de Vries, E. Portolés, G. Zheng, T. Taniguchi, K. Watanabe, T. Ihn, K. Ensslin, and P. Rickhaus, "Gate-defined josephson junctions in magic-angle twisted bilayer graphene," *Nature Nanotechnology*, pp. 1–4, 2021.

[10] X. Liu, Z. Wang, K. Watanabe, T. Taniguchi, O. Vafek, and J. Li, "Tuning electron correlation in magic-angle twisted bilayer graphene using coulomb screening," *Science*, vol. 371, no. 6535, pp. 1261–1265, 2021.

[11] D. Wong, K. P. Nuckolls, M. Oh, B. Lian, Y. Xie, S. Jeon, K. Watanabe, T. Taniguchi, B. A. Bernevig, and A. Yazdani, "Cascade of electronic transitions in magic-angle twisted bilayer graphene," *Nature*, vol. 582, no. 7811, pp. 198–202, 2020.

[12] P. Stepanov, M. Xie, T. Taniguchi, K. Watanabe, X. Lu, A. H. MacDonald, B. A. Bernevig, and D. K. Efetov, "Competing zero-field chern insulators in superconducting twisted bilayer graphene," *arXiv preprint arXiv:2012.15126*, 2020.

[13] U. Zondiner, A. Rozen, D. Rodan-Legrain, Y. Cao, R. Queiroz, T. Taniguchi, K. Watanabe, Y. Oreg, F. von Oppen, A. Stern, *et al.*, "Cascade of phase transitions and dirac revivals in magic-angle graphene," *Nature*, vol. 582, no. 7811, pp. 203–208, 2020.

[14] Y. Saito, F. Yang, J. Ge, X. Liu, T. Taniguchi, K. Watanabe, J. Li, E. Berg, and A. F. Young, "Isospin pomeranchuk effect in twisted bilayer graphene," *Nature*, vol. 592, no. 7853, pp. 220–224, 2021.

[15] Y. Cao, J. M. Park, K. Watanabe, T. Taniguchi, and P. Jarillo-Herrero, "Pauli-limit violation and re-entrant superconductivity in moiré graphene," *Nature*, vol. 595, no. 7868, pp. 526–531, 2021.

[16] Y. Choi, H. Kim, C. Lewandowski, Y. Peng, A. Thomson, R. Polski, Y. Zhang, K. Watanabe, T. Taniguchi, J. Alicea, *et al.*, "Interaction-driven band flattening and correlated phases in twisted bilayer graphene," *arXiv preprint arXiv:2102.02209*, 2021.

[17] Y. Choi, H. Kim, Y. Peng, A. Thomson, C. Lewandowski, R. Polski, Y. Zhang, H. S. Arora, K. Watanabe, T. Taniguchi, *et al.*, "Correlation-driven topological phases in magic-angle twisted bilayer graphene," *Nature*, vol. 589, no. 7843, pp. 536–541, 2021.

[18] Supplementary-materials

[19] M. Serlin, C. Tschirhart, H. Polshyn, Y. Zhang, J. Zhu, K. Watanabe, T. Taniguchi, L. Balents, and A. Young, "Intrinsic quantized anomalous hall effect in a moiré heterostructure," *Science*, vol. 367, no. 6480, pp. 900–903, 2020.

[20] A. L. Sharpe, E. J. Fox, A. W. Barnard, J. Finney, K. Watanabe, T. Taniguchi, M. Kastner, and D. Goldhaber-Gordon, "Emergent ferromagnetism near three-quarters filling in twisted bilayer graphene," *Science*, vol. 365, no. 6453, pp. 605–608, 2019.

[21] K. Levin and O. T. Valls, "Phenomenological theories of liquid

3he," *Physics Reports*, vol. 98, no. 1, pp. 1–56, 1983.

[22] P. W. Anderson and W. Brinkman, "Anisotropic superfluidity in he 3: A possible interpretation of its stability as a spin-fluctuation effect," *Physical Review Letters*, vol. 30, no. 22, p. 1108, 1973.

[23] N. Berk and J. Schrieffer, "Effect of ferromagnetic spin correlations on superconductivity," *Physical Review Letters*, vol. 17, no. 8, p. 433, 1966.

[24] It is also true that attractive intersublattice interactions $\Gamma^{AB} < 0$ produce superconductivity when the intrasublattice interaction is repulsive. See [18] for a discussion of this case.

[25] P. Anderson and W. Brinkman, "Theory of anisotropic superfluidity in he3," in *Basic Notions of Condensed Matter Physics*, pp. 287–388, CRC Press, 2018.

[26] A. H. MacDonald, J. Jung, and F. Zhang, "Pseudospin order in monolayer, bilayer and double-layer graphene," *Physica Scripta*, vol. 2012, no. T146, p. 014012, 2012.

[27] J. Velasco, L. Jing, W. Bao, Y. Lee, P. Kratz, V. Aji, M. Bockrath, C. Lau, C. Varma, R. Stillwell, *et al.*, "Transport spectroscopy of symmetry-broken insulating states in bilayer graphene," *Nature nanotechnology*, vol. 7, no. 3, pp. 156–160, 2012.

[28] G. Vignale and K. Singwi, "Effective two-body interaction in coulomb fermi liquids," *Physical Review B*, vol. 32, no. 4, p. 2156, 1985.

[29] N. Bickers, "Self-consistent many-body theory for condensed matter systems," in *Theoretical Methods for Strongly Correlated Electrons*, pp. 237–296, Springer, 2004.

[30] M. Nava, A. Motta, D. Galli, E. Vitali, and S. Moroni, "Equation of state of two-dimensional 3 he at zero temperature," *Physical Review B*, vol. 85, no. 18, p. 184401, 2012.

[31] P. W. Anderson, "Heavy-electron superconductors, spin fluctuations, and triplet pairing," *Phys. Rev. B*, vol. 30, pp. 1549–1550, Aug 1984.

[32] We use crossing-symmetry [29] to relate the vertex functions in the particle-particle channel (Λ_P) to the one in particle-hole channel (Λ).

[33] When the filling factor ν approaches $\nu = -3$, the enhanced valley polarizability not only generates a valley-singlet repulsion but also an attraction between electrons in the same valley. When this attraction leads to condensation of Cooper pairs from the same valley, the resulting superconducting order parameter cannot be uniform-s-wave because of Fermi statistics. (We assume the normal state is always spin-polarized). This means the order parameter might undergo a transition from valley-singlet to valley-triplet as $\nu \to -3$ and might explain the $U - V$ transition recently observed in local-tunneling spectroscopy [**?**]. In this scenario, valley-triplet superconductivity close to $\nu = -3$ is eventually suppressed by the enhanced pair-breaking (trigonal-warping) potential from the band-Hamiltonian.

[34] P. Stepanov, I. Das, X. Lu, A. Fahimniya, K. Watanabe, T. Taniguchi, F. H. Koppens, J. Lischner, L. Levitov, and D. K. Efetov, "Untying the insulating and superconducting orders in magic-angle graphene," *Nature*, vol. 583, no. 7816, pp. 375–378, 2020.

[35] H. S. Arora, R. Polski, Y. Zhang, A. Thomson, Y. Choi, H. Kim, Z. Lin, I. Z. Wilson, X. Xu, J.-H. Chu, *et al.*, "Superconductivity in metallic twisted bilayer graphene stabilized by wse 2," *Nature*, vol. 583, no. 7816, pp. 379–384, 2020.

[36] T. Cea, N. R. Walet, and F. Guinea, "Electronic band structure and pinning of fermi energy to van hove singularities in twisted bilayer graphene: A self-consistent approach," *Phys. Rev. B*, vol. 100, p. 205113, Nov 2019.

[37] F. Guinea and N. R. Walet, "Electrostatic effects, band distortions, and superconductivity in twisted graphene bilayers," *Proceedings of the National Academy of Sciences*, vol. 115, no. 52, pp. 13174–13179, 2018.

[38] M. Xie and A. H. MacDonald, "Weak-field hall resistivity and spin/valley flavor symmetry breaking in matbg," *arXiv preprint arXiv:2010.07928*, 2020.

[39] Y. W. Choi and H. J. Choi, "Strong electron-phonon coupling, electron-hole asymmetry, and nonadiabaticity in magic-angle twisted bilayer graphene," *Physical Review B*, vol. 98, no. 24, p. 241412, 2018.

[40] F. Wu, A. MacDonald, and I. Martin, "Theory of phonon-mediated superconductivity in twisted bilayer graphene," *Physical review letters*, vol. 121, no. 25, p. 257001, 2018.

[41] W. Qin, B. Zou, and A. H. MacDonald, "Critical magnetic fields and electron-pairing in magic-angle twisted bilayer graphene," *arXiv preprint arXiv:2102.10504*, 2021.

[42] D. Abanin and L. Levitov, "Quantized transport in graphene pn junctions in a magnetic field," *Science*, vol. 317, no. 5838, pp. 641–643, 2007.

[43] E. Codecido, Q. Wang, R. Koester, S. Che, H. Tian, R. Lv, S. Tran, K. Watanabe, T. Taniguchi, F. Zhang, *et al.*, "Correlated insulating and superconducting states in twisted bilayer graphene below the magic angle," *Science advances*, vol. 5, no. 9, p. eaaw9770, 2019.

[44] R. Ojajärvi, T. Hyart, M. A. Silaev, and T. T. Heikkilä, "Competition of electron-phonon mediated superconductivity and stoner magnetism on a flat band," *Physical Review B*, vol. 98, no. 5, p. 054515, 2018.

[45] T. Cea and F. Guinea, "Coulomb interaction, phonons, and superconductivity in twisted bilayer graphene," *Proceedings of the National Academy of Sciences*, vol. 118, no. 32, 2021.

[46] H. Zhou, T. Xie, T. Taniguchi, K. Watanabe, and A. F. Young, "Superconductivity in rhombohedral trilayer graphene," *arXiv preprint arXiv:2106.07640*, 2021.

[47] H. Zhou, L. Holleis, Y. Saito, L. Cohen, W. Huynh, C. L. Patterson, F. Yang, T. Taniguchi, K. Watanabe, and A. F. Young, "Isospin magnetism and spin-polarized superconductivity in bernal bilayer graphene," *Science*, vol. 375, no. 6582, pp. 774–778, 2022.

[48] Y. Zhang, R. Polski, A. Thomson, É. Lantagne-Hurtubise, C. Lewandowski, H. Zhou, K. Watanabe, T. Taniguchi, J. Alicea, and S. Nadj-Perge, "Spin-orbit enhanced superconductivity in bernal bilayer graphene," *arXiv preprint arXiv:2205.05087*, 2022.

[49] W. Qin, C. Huang, T. Wolf, N. Wei, I. Blinov, and A. H. MacDonald, "Functional renormalization group study of superconductivity in rhombohedral trilayer graphene," *arXiv preprint arXiv:2203.09083*, 2022.

[50] W. Q. N. W. I. B. M. A. H. Chunli Huang, Tobias Wolf, "Spin and orbital metallic magnetism in rhombohedral trilayer graphene," *arXiv preprint arXiv:2203.12723*, 2022.